AIAA JOURNAL
Vol. 33, No. 9, September 1995

Buckling and Postbuckling of Spherical Shells with Apical Cutout Under Ring Load

Ming-Chyuan Lin* and Meng-Kao Yeh†
National Tsing Hua University, Hsinchu 30043, Taiwan, Republic of China

The buckling and postbuckling behavior of elastoplastic spherical shells with circular apical cutout under a ring load was investigated analytically and experimentally. A finite element code based on the updated Lagrangian formulation was established to analyze this buckling problem by considering nonlinear geometric and material properties. An iterative scheme controlled by displacement was adopted in the solution procedure to avoid numerical instability near the limit buckling load. Ring loads of both line and strip types were analyzed. A testing device was used to perform buckling experiments. The ratio of diameter to thickness of the steel specimens was between 30.23 and 86.75. The influence of the ratio of diameter to thickness and the sizes of the apical cutout and ring load on the limit buckling load are discussed. The analytical results agree satisfactorily with experimental ones for medium-carbon steel spherical shells. Convex and concave modes of postbuckling deformation around the apex are obtained in analysis and observed in experiment for varied combinations of the sizes of ring load and apical cutout and ratio of diameter to thickness of the spherical shells.

Introduction

SPHERICAL shells are commonly used in engineering structures, such as missiles, aircrafts, and pressure vessels in nuclear and chemical industries. During their service life, these structures are subjected to loads of various types. Previous works about the buckling and postbuckling behavior of spherical shells under ring loads are few. A concentrated load at the apex can be treated as a special case of ring load. In past investigations of the stability of spherical shells under concentrated load, only elastic spherical shells were discussed. Mescall[1] analyzed the large-deflection behavior of spherical shells under a concentrated load; he established an approximate empirical relationship between the critical load and a geometric parameter of the elastic spherical shell. Penning[2] tested the elastic stability of clamped aluminum shallow shells under a load of small but finite area at the apex; he found a critical geometric parameter below which the unbuckled shell exhibited plastic behavior. Bushnell[3] found that the analytical outward-directed point load at buckling was 18–24 times the critical inward-directed point load for elastic shallow spherical shells. Fitch[4] investigated asymmetric buckling of clamped elastic shallow spherical shells under a concentrated load according to perturbation method. Brodland and Cohen[5] examined buckling and postbuckling behavior of simply supported shallow and full hemispherical rubber caps under a point load. Nowinka and Lukasiewicz[6] investigated analytically the load-deflection responses of spherical shells under an apical point load with two axially symmetric elements. The elastic buckling of shallow spherical shells under a point load and external pressure was investigated by Loo and Evan-Iwanowski[7] and by Holston.[8] The load-deflection response of fluid-filled rubber hemispherical shells under a point load was examined analytically and experimentally by Taber.[9]

For buckling of spherical shells under a ring load, Evan-Iwanowski et al.[10] tested elastic shallow spherical shells and found that the radius of the ring load affected the buckling loads. Cagan and Taber[11] analyzed the buckling and postbuckling behavior of elastic spherical shells. Xie et al.[12] examined numerically the buckling of a truncated elastic shallow spherical shell, with a rigid inclusion at the cutout, subjected to combined ring load on the edge of the cutout and external pressure on the shallow shells. Gu[13,14] analyzed the effects of the radius of the ring load and the radius and edge reinforcement of the central circular cutout on the buckling behavior of elastic shallow spherical shells; he found that, beyond a critical value of the ratio between the radius of the ring load to the radius of the shallow shell base, the load increased again to the buckling load of the same shell under a point load after decreasing from a maximum of the load-deflection response. Bushnell[3] established an approximate formula for the buckling load of an outward-directed ring load on elastic spherical shells. However, reports of the elastoplastic buckling of spherical shells under ring load are lacking.

In this work, we considered an elastoplastic material and established a finite element code based on the updated Lagrangian formulation[15,16] to analyze the buckling and postbuckling behavior of clamped spherical shells with a circular apical cutout under ring load. Ring loads of both line and strip types were analyzed, of which the strip type was not previously investigated. An incremental displacement-controlled scheme[17] was adopted to avoid divergence near the buckling load. The analytical results are compared with experimental ones for medium-carbon steel spherical shells. The influence of the ratio of diameter to thickness and the sizes of the circular cutout and of the ring load on the buckling load and postbuckling mode of elastoplastic hemispherical shells are described. Convex and concave modes of postbuckling deformation around the apex of the spherical shell are obtained in analysis and observed in experiment.

Updated Lagrangian Formulation

Since the shell surface undergoes large displacements and large rotations for the buckling problem, the updated Lagrangian formulation was adopted to treat this nonlinear geometrical problem. As the body moves and deforms from original configuration O to the current configuration S, all variables and the equilibrium of the body in the current configuration S are known and are used to obtain the next required equilibrium configuration T. The linearized equilibrium equation of the problem was derived from the principle of virtual work[15] as

$$\int_V C_{ijrs} e_{rs} \delta e_{ij}\, dV + \int_V \tau_{ij} \delta \eta_{ij}\, dV = \int_{T_A} {}^T P_i \delta u_i\, dA - \int_V \tau_{ij} \delta e_{ij}\, dV \tag{1}$$

in which C_{ijrs} is the elasticity tensor, e_{ij} and η_{ij} are the linear and nonlinear parts of the strain increment tensor, τ_{ij} is the Cauchy stress tensor, and u_i is the displacement at the point where external force ${}^T P_i$ is applied. All of these tensors were considered in the current configuration S, whereas the external force ${}^T P_i$ was referred to the next required configuration T.

Received Nov. 18, 1994; revision received Feb. 17, 1995; accepted for publication Feb. 20, 1995.

*Graduate Student, Department of Power Mechanical Engineering.
†Associate Professor, Department of Power Mechanical Engineering. Member AIAA.

Finite Element Method

The degenerated shell element[18] with eight nodal points was used to discretize the continuous system. This element geometry was interpolated using coordinates and normals of the midsurface nodal point. We assumed that lines originally normal to the midsurface of the shell remained straight during the element deformation and that no transverse normal stress was developed. The coordinate of a generic point in the shell element undergoing a large displacement and rotation was interpolated as

$$\boldsymbol{X} = \sum_{k=1}^{8} N_k \boldsymbol{X}^k + \frac{\zeta}{2} \sum_{k=1}^{8} a_k N_k \boldsymbol{V}^k \tag{2}$$

in which $N_k = N_k(r, s, t)$ is the shape function at nodal point k based on orthogonal natural coordinates (r, s, t) for the element, $\boldsymbol{X}^k$ is the local coordinate of nodal point k, ζ is the local coordinate in the thickness direction, a_k is the thickness at the nodal point k, and $\boldsymbol{V}^k$ is the unit normal vector to the midsurface at nodal point k.

The incremental displacement $\boldsymbol{U}_e$ of a generic point in this element from configuration S to configuration T is expressed as

$$\boldsymbol{U}_e = \sum_{k=1}^{8} N_k \boldsymbol{U}^k + \frac{\zeta}{2} \sum_{k=1}^{8} a_k N_k \left[-\boldsymbol{V}_2{}^k \alpha_k + \boldsymbol{V}_1{}^k \beta_k \right] \tag{3}$$

in which $\boldsymbol{U}^k = (u_r^k, u_s^k, u_t^k)$ is the incremental displacement at nodal point k, α_k and β_k are rotations along the directions $\boldsymbol{V}_1^k$ and $\boldsymbol{V}_2^k$, which form a set of orthogonal vectors with $\boldsymbol{V}^k$. There are five degrees of freedom, $u_r^k, u_s^k, u_t^k, \alpha_k$ and β_k, for each nodal point. With a coordinate transformation between local coordinates (r, s, t) and global Cartesian coordinates (x, y, z), the equilibrium equation (1) can be expressed in the following form in global coordinates for each element as

$$\{[K]_l + [K]_{nl}\}\boldsymbol{U}_e = {}^T\boldsymbol{P}_e - \boldsymbol{F}_e \tag{4}$$

in which

$$[K]_l = \int_V [B]_L^T [C][B]_L \, dV \tag{5}$$

$$[K]_{nl} = \int_V [B]_{NL}^T [\tau][B]_{NL} \, dV \tag{6}$$

$$F_e = \int_V [B]_L^T \tau \, dV \tag{7}$$

In Eqs. (4–7), $[K]_l$ and $[K]_{nl}$ are linear and nonlinear parts of the element stiffness matrices, $[B]_L$ and $[B]_{NL}$ are the corresponding linear and nonlinear strain-displacement transformation matrices, $[C]$ is the material property matrix, $[\tau]$ and τ are the Cauchy stress matrix and stress vector, ${}^T\boldsymbol{P}_e$ is the effective force vector in the configuration T, and $\boldsymbol{F}_e$ is the internal nodal force vector.

Assembling the element equilibrium equation (4), we express the global system equilibrium equation as

$$\{[K]_L + [K]_{NL}\}\boldsymbol{U} = {}^T\boldsymbol{P} - \boldsymbol{F} \tag{8}$$

in which $[K]_L$ and $[K]_{NL}$ are the linear and nonlinear parts of the global stiffness matrix, $\boldsymbol{U}$ is the global displacement incremental vector from the current configuration S to the next required configuration T, ${}^T\boldsymbol{P}$ is the global effective applied force vector in configuration T, and $\boldsymbol{F}$ is the internal force vector in configuration S.

Elastoplastic Materials

The specimens used in the buckling experiment were made of medium-carbon steel (AISI 1045). A typical axial stress-strain curve showed bilinear characteristics for strain less than 5%. We used a bilinear equation to fit the uniaxial stress-strain curve, although other fitting equations can be implemented in the analysis[17]:

$$\varepsilon = \begin{cases} \sigma/E & \text{if } \sigma \le \sigma_y \\ \sigma_y/E + (\sigma - \sigma_y)/E_p & \text{if } \sigma > \sigma_y \end{cases} \tag{9}$$

in which ε and σ are the axial strain and stress, E is Young's modulus, σ_y is the yield stress, and E_p is the second modulus for the material in the plastic range.

If the material remains elastic, the property matrix $[C_e]$ of the elastic material, under the assumption that the stress normal to the shell midsurface remains zero, is

$$[C_e] = \frac{E}{(1-\nu^2)} \begin{bmatrix} 1 & \nu & 0 & 0 & 0 & 0 \\ \nu & 1 & 0 & 0 & 0 & 0 \\ 0 & 0 & 0 & 0 & 0 & 0 \\ 0 & 0 & 0 & \dfrac{1-\nu}{2} & 0 & 0 \\ 0 & 0 & 0 & 0 & \dfrac{1-\nu}{2(1.2)} & 0 \\ 0 & 0 & 0 & 0 & 0 & \dfrac{1-\nu}{2(1.2)} \end{bmatrix} \tag{10}$$

in which ν is Poisson's ratio. The factor 1.2 is included in the matrix to correct the uniform shear stress assumption through the thickness direction.[19]

For the plastic material, we assumed that under a multiaxial stress state the effective stress-strain relation was equivalent to the uniaxial stress-strain relation. The isotropic hardening rule was used for further yield of the material based on the J_2 flow theory:

$$F(\sigma) = \sqrt{3J_2} - \sigma_{\max} = 0 \tag{11}$$

in which $\sqrt{3J_2}$ is the effective stress, $\sigma_{\max}$ represents the greatest value of σ during the loading history. The initial value of $\sigma_{\max}$ used in the analysis was σ_y. With Eq. (11), we assessed whether further loading occurs for each Gaussian integration point in the process of forming the stiffness matrix. For the material loaded beyond the yielding surface, the property matrix $[C_{ep}]$ of the elastoplastic material must be used:

$$[C_{ep}] = [C_e] - \frac{[C_e]\{a\}\left(\{a\}^T[C_e]\right)}{H_p + \{a\}^T[C_e]\{a\}} \tag{12}$$

in which

$$\{a\} = \frac{\partial F(\sigma)}{\partial \sigma} \tag{13}$$

$$H_p = EE_p/(E - E_p) \tag{14}$$

If unloading occurred in the incremental loading process, the elastic material property matrix $[C_e]$ was used. The material property matrices $[C_e]$ or $[C_{ep}]$ were used in Eq. (5) for each Gaussian integration point to obtain the element stiffness matrices.

Displacement Controlled Incremental Procedure

In solving the problem, the system equilibrium equation (8) is expressed in an iterative form[15–17] as

$$\{[K]_L + [K]_{NL}\}\boldsymbol{U}^{(i)} = {}^T\boldsymbol{P}^{(i)} - {}^T\boldsymbol{F}^{(i-1)} \tag{15}$$

in which i represents the iteration index. In Eq. (15), $[K]_L$ and $[K]_{NL}$ were updated in each incremental step, and ${}^T\boldsymbol{F}^{(i-1)}$ was calculated based on the prior state $i-1$.

As the effective external force vector ${}^T\boldsymbol{P}^{(i)}$ was difficult to predict, especially for the shell under a ring load of strip type, a scheme controlled by displacement[17] was used to overcome this problem and to avoid numerical instability near the buckling point. The displacements where the ring load of line or strip type was applied on the spherical shell were used as the controlling increment whereas the base of the shell was clamped. Besides the ring load and the reaction on the clamped base, the shell was free of traction. In each increment, the known controlling displacements were eliminated from the displacement vector $\boldsymbol{U}^{(i)}$ with proper modification made to the stiffness matrix and external force vector. Then the condensed form of the equilibrium equation is

$$\{[K]_{LC} + [K]_{NLC}\}\boldsymbol{U}_C^{(i)} = {}^T\boldsymbol{P}_C^{(i)} - {}^T\boldsymbol{F}_C^{(i-1)} \tag{16}$$

in which subscript C implies "condensed." Thus, all entries of $U_C^{(i)}$ are unknown, and all entries of ${}^T P_C^{(i)}$ and ${}^T F_C^{(i-1)}$ are known. $U_C^{(i)}$ was easily solved, and ${}^T P^{(i)}$ in Eq. (15) was calculated thereafter. Then the ring load applied to the shell was obtained. As Eq. (16) is of an iterative form, the modified Newton–Raphson iterative method was adopted; the iterative process was terminated only when the following convergence criteria were satisfied:

$$\frac{\|U_C^{(i)}\|}{\|\sum_i U^{(i)}\|} < \varepsilon_D \quad \text{and} \quad \frac{\|{}^T P_C^{(i)} - {}^T F_C^{(i-1)}\|}{\|{}^T P_C^{(i)} - {}^T F_C^{(0)}\|} < \varepsilon_D \qquad (17)$$

in which ε_D is a chosen tolerance for convergence, 0.001. The total displacement vector ${}^T U$ in the required configuration T was obtained as

$${}^T U = {}^S U + \sum_i U^{(i)} \qquad (18)$$

in which ${}^S U$ is the displacement vector in the current configuration S.

Experiments

A testing machine was used to perform the buckling experiment on clamped hemispherical shells. A load cell and one displacement transducer were used to measure the loads and the corresponding displacements of the tested spherical shells, respectively. The signals of the load cell and the displacement transducer were amplified and fed into a data-acquisition card built into a microcomputer to obtain the load-deflection responses of the specimens.

The specimens used in the buckling experiment were made of medium-carbon steel (AISI 1045). The geometry of the spherical shell specimen is shown in Fig. 1, in which D and t are the medium diameter and thickness of the shell; H is the depth clamped during the buckling experiment; d is the diameter of the circular cutout at the apex; c, b, and L are the outer diameter, thickness, and length of the loading ring, respectively.

The thickness of the specimens was measured with a micrometer. The mean radius of the spherical shells was measured on a rotating plate fixed to a milling machine. The average mean diameter D of the specimens was 144 mm; the average thickness of the four groups of specimens were 1.660, 2.587, 3.688, and 4.763 mm, respectively. The diameter of the circular apical cutout of these four groups were $d = 30$ mm. To examine the effect of the size of the circular cutout, we used a specimen group of thickness $t = 2.587$ mm with diameters $d = 0$, 20, 30, 40, 50, and 70 mm of the cutout. The loading ring had outer diameter $c = 80$ mm, thickness $b = 5$ mm, length $L = 50$ mm and was welded onto each specimen along the outer junction line; therefore, all tested specimens had ring loads of strip type rather than line type. Since the loading rings were thick enough and welded onto the specimens, no buckling occurred on these loading rings and a downward displacement was ensured for the ring-loaded area on specimens during the experiment.

Four strip specimens were made from the same material to evaluate the material parameters. A typical axial stress-strain curve showed bilinear characteristics for medium-carbon steel (AISI 1045) with strain less than 5%; Eq. (9) was used to describe this stress-strain relationship. The average material parameters obtained are $E = 184 \pm 10$ Gpa, $\sigma_y = 266 \pm 9$ Mpa, $E_p = 0.368 \pm 0.020$ Gpa, and $\nu = 0.286 \pm 0.012$. All of these parameters were used in the numerical analysis.

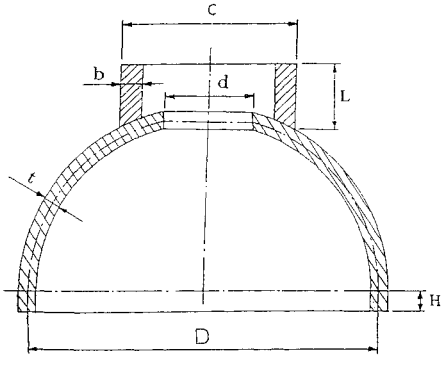

Fig. 1 Geometry of the spherical shell specimen.

Results and Discussion

In the present work, we are interested in an elastoplastic hemispherical shell under a ring load. Whole hemispherical shell can be analyzed for the symmetric and asymmetric buckling and postbuckling deformation. Since no asymmetric buckling modes were observed in our experiments and in the work performed by Evan-Iwanwski et al.,[10] only one-quarter of each shell was analyzed for the axially symmetric buckling deformation. The analytical model was first verified for buckling loads of elastic shallow spherical shells of diameter $D = 508$ mm and rise $h/D = 0.01545$ under a ring load of line type ($c/D = 0.1$) for varied thickness $t = 0.254$, 0.381, and 0.5334 mm as shown in Fig. 2. The material properties of these shells are Young's modulus $E = 2.96$ GPa and Poisson's ratio $\nu = 0.33$. The ring load at buckling F_b was made dimensionless with $2Et^3/D$. The dimensionless buckling loads increased as the ratio of diameter to thickness D/t increased. The analytical results agreed satisfactorily with results of experiments by Evan-Iwanowski et al.[10]

For a hemispherical shell of diameter $D = 144$ mm and thickness $t = 2.587$ mm, the analytical load-deflection responses of elastic ($E = 184$ GPa) and elastoplastic ($E = 184$ Gpa, $E_p = 0.368$ Gpa) shells with a circular apical cutout ($d/D = 0.208$) under ring load of line type ($c/D = 0.208$, $b = 0$) are shown in Fig. 3. The load F and displacement w at the place where the load is applied are used as ordinate and abscissa with dimensionless factors $2Et^3/D$ and $D/2$, respectively. The limit buckling load occurred for both elastic and elastoplastic shells with a circular apical cutout. In the postbuckling region, the load increased again after a minimum load was attained. The response of the elastoplastic shell was much less than that of the elastic one; therefore, it is necessary to consider the elastoplastic behavior of the material for thicker spherical shells. The shell without cutout is a special case of shell with cutout $d = 0$. A limit buckling load occurred for neither elastic nor elastoplastic

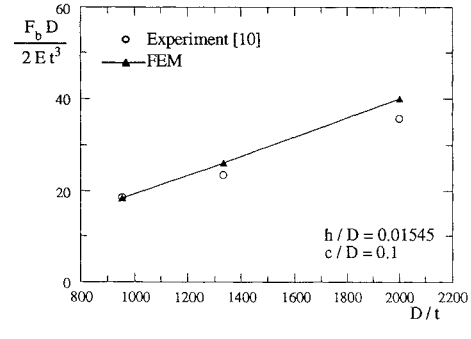

Fig. 2 Buckling loads of elastic shallow spherical shells under ring load for varied ratios of diameter to thickness.

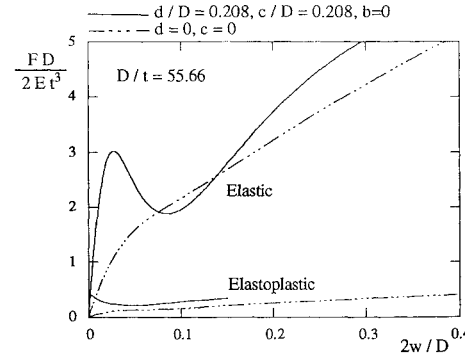

Fig. 3 Load-deflection responses of elastic and elastoplastic hemispherical shells under ring load and point load at apex.

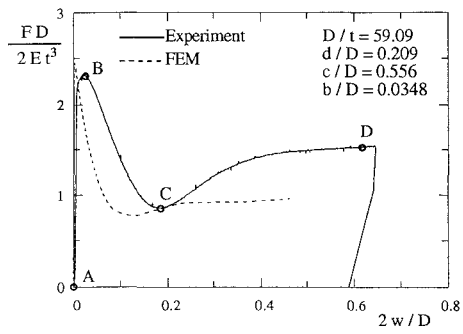

Fig. 4 Analytical and experimental responses of elastoplastic hemispherical shells with a circular apical cutout under a ring load of strip type.

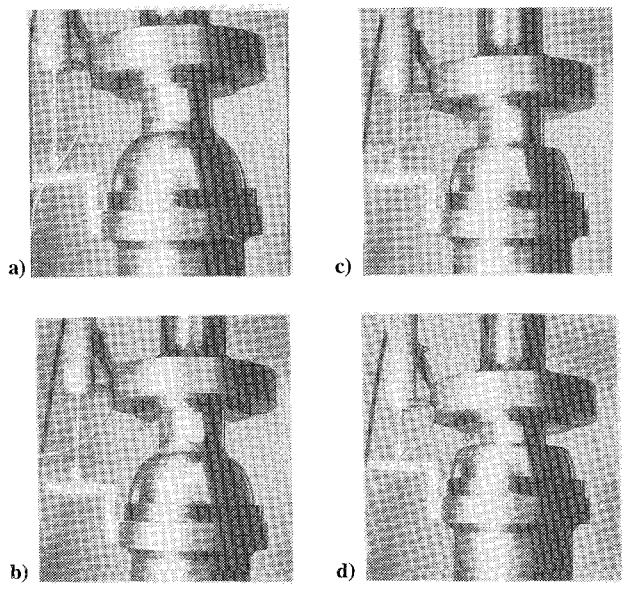

Fig. 5 Progressive deformation of an elastoplastic hemispherical shell with a circular apical cutout under a ring load of strip type.

shell without cutout when the ring load shrank to an apical point load. Their analytical responses are shown in Fig. 3 for comparison.

Typical load-deflection responses obtained from analysis and experiment for a hemispherical shell (D = 144 mm, D/t = 59.09) with a circular apical cutout (d/D = 0.209) under a ring load of strip type (c/D = 0.556, b/D = 0.0348) appear in Fig. 4. The analytical response has a trend similar to, but is steeper than, the experimental one. The dimensionless analytical buckling load was 2.453, whereas the experimental one was 2.343. Figure 5 shows the experimental progressive deformation corresponding to states A, B, C, and D in Fig. 4. As shown in Fig. 5b, the shell began to bulge as the limit buckling 86.38 kN was attained (point B in Fig. 4). Then the ring load decreased to a minimum 31.72 kN (point C in Fig. 4), and the ring-loaded area of the shell collapsed as shown in Fig. 5c. As the experiment continued, the ring load increased again slowly and the deformation became more severe as shown in Fig. 5d. The experiment stopped when the ring-loaded part reached the bottom support of the shell specimen. This collapsed specimen with a convex apical portion is shown in Fig. 6a. A concave deformation of another thicker specimen (D/t = 30.23, d/D = 0.208, c/D = 0.556, b/D = 0.0347) is shown in Fig. 6b.

Convex and Concave Postbuckling Modes

Figure 7 shows the convex and concave progressive postbuckling deformation from analysis of elastoplastic hemispherical shells with D/t = 55.66, d/D = 0.208. The dashed lines in Fig. 7 represent the original shape of the shells, and the solid lines closest to the dashed lines represent the shell shapes at buckling. The convex postbuckling mode for c/D = 0.556 (Fig. 7a) with part of the shell outside the

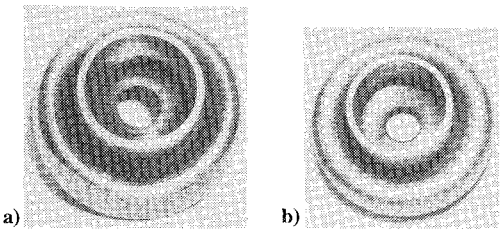

Fig. 6 Convex and concave postbuckling deformation of shell specimens.

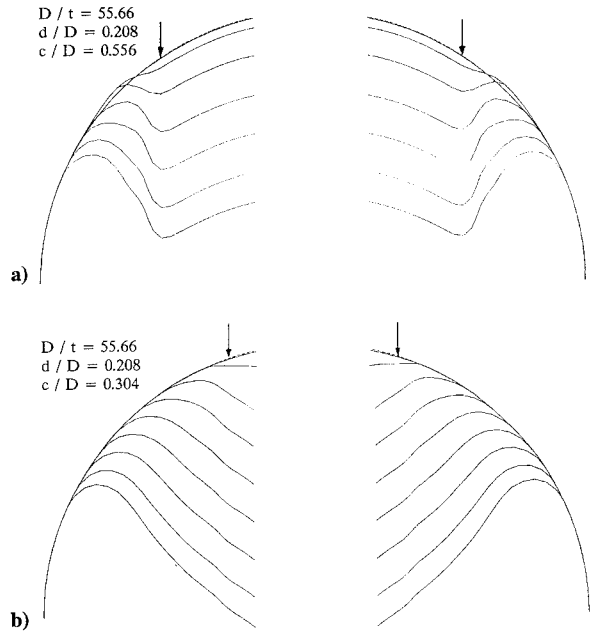

Fig. 7 Analytical progressive deformation for hemispherical shells with a circular apical cutout under a ring load of line type.

loading ring of line type bulging was observed in experiment as shown in Fig. 6a. The concave postbuckling mode for c/D = 0.304 (Fig. 7b) was similar to the mode observed in experiment as shown in Fig. 6b. For shells under ring load of line type (b = 0), the convex mode occurred for cases with $c/D \geq 0.420$, whereas the concave mode occurred for cases with $c/D < 0.420$. All analytical results for a ring load of strip type showed only the convex mode because of constraints on the ring-loaded region.

A shell without a cutout is a special case of a shell with diameter of cutout d = 0. The convex and concave modes were also obtained for a shell without a cutout as shown in Fig. 8. For the shell of D/t = 55.66, the convex mode occurred for $c/D \geq 0.342$, whereas the concave mode occurred for $c/D < 0.342$. The existence of the apical cutout (d/D = 0.208) made the convex mode occur for larger loading ring ($c/D \geq 0.420$) when compared with a shell without cutout ($c/D \geq 0.342$).

The size of the circular cutout also affected the postbuckling deformation of spherical shells. When D/t = 55.66 and c/D = 0.556, the convex mode occurred for shells under a ring load of line type (b = 0) with a circular cutout of smaller diameter ($d/D < 0.420$), and the concave mode occurred for shells with a circular cutout of larger diameter ($d/D \geq 0.420$). The experimental results of the same shells (D/t = 55.66, c/D = 0.556) under ring loads of strip type (b/D = 0.0347) showed the convex mode for $d/D \leq 0.208$ and the concave mode for $d/D \geq 0.278$. Since the loading in experiment was of strip type before buckling, the experimental d/D value of the transition from convex to concave mode was smaller than the analytical one.

The D/t value also had effects on the transition from the convex to the concave mode for spherical shells. In particular, for d/D = 0.208, c/D = 0.556, b = 0, the convex mode occurred for thin shells ($D/t \geq 30.5$) and the concave mode for thick shells ($D/t < 30.5$). The shells (d/D = 0.208) under ring loads of strip type

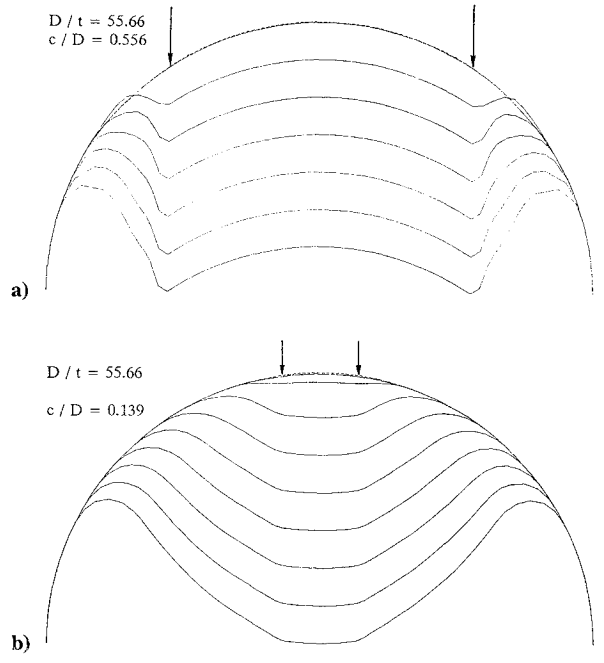

Fig. 8 Analytical progressive deformation for hemispherical shells under a ring load of line type.

($c/D = 0.556$, $b/D = 0.0347$) exhibited experimentally the convex mode for $D/t \geq 55.66$ and the concave mode for $D/t \leq 39.05$; due to ring load of strip type, the shells deformed more easily into the concave mode for thinner shells than in the analytical results. Therefore, the convex postbuckling mode occurred for thinner shells and shells of larger diameter of ring load and with smaller apical cutout.

Effect of Ratio of Diameter to Thickness on Shell Behavior

The analytical and experimental results of elastoplastic hemispherical shells ($D = 144$ mm) with a circular apical cutout ($d/D = 0.208$) under ring load ($c/D = 0.556$) are shown in Fig. 9 for various ratios of diameter to thickness. The buckling load F_b was made dimensionless with $2Et^3/D$. The analytical results obtained for ring loads of line type ($b = 0$) and strip type ($b/D = 0.0347$) were similar. The dimensionless buckling load increased as the ratio of diameter to thickness (D/t) increased. According to Fig. 9, the analytical buckling load agreed satisfactorily with experimental data.

Effect of Size of Circular Apical Cutout on Shell Behavior

The analytical and experimental results of elastoplastic hemispherical shells ($D/t = 55.66$) under ring load ($c/D = 0.556$) with varied diameters of the circular apical cutout are shown in Fig. 10. The analytical results were obtained for ring loads of both line ($b = 0$) and strip ($b/D = 0.0347$) types. The analytical buckling loads from analysis of a ring load of strip type were almost constant in the range of the diameter of apical cutout from $d/D = 0$ to 0.486. The ring load was supported mostly by part of the shell outside the load ring. When the edge of the apical cutout was far from the region of the ring load, the analytical results for shells under ring load of line type were equal to those under ring load of strip type. When the edge of the apical cutout was near the ring load of line type, the material used to support the loads was less and the buckling loads decreased slightly, as shown in Fig. 10 for $d/D = 0.486$ and 0.556. Therefore, the buckling load of shell under a ring load of strip type can be analyzed with a ring load of line type as long as the edge of the cutout is far from the region of the ring load. As the average ratio of diameter to thickness was used in analysis, the experimental results scattered near the analytical ones due to small variations in the ratio of diameter to thickness for each specimen.

Effect of Diameter of Ring Load on Shell Behavior

Figure 11 shows the analytical load-deflection responses of elastoplastic hemispherical shells ($D = 144$ mm, $D/t = 55.66$) with a circular apical cutout ($d/D = 0.208$) under varied diameter

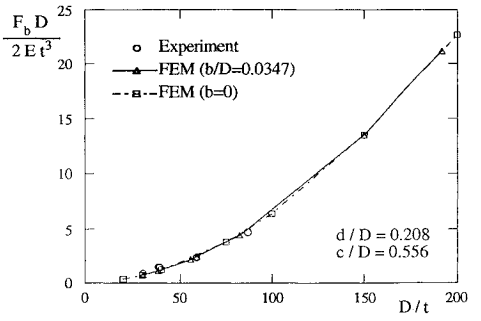

Fig. 9 Analytical and experimental buckling loads of hemispherical shells with a circular apical cutout under ring loads for varied ratios of diameter to thickness.

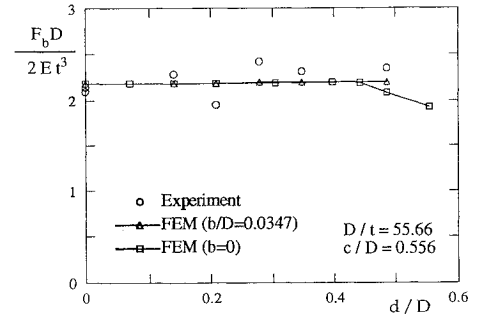

Fig. 10 Analytical and experimental buckling loads of hemispherical shells under ring loads for varied size of circular apical cutout.

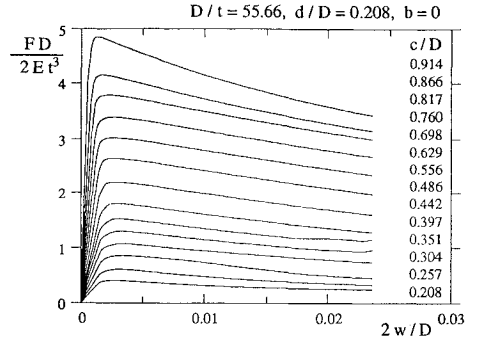

Fig. 11 Analytical load-deflection responses of hemispherical shells with a circular apical cutout under varied ring loads of line type.

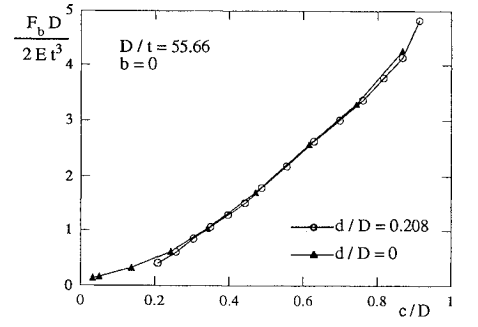

Fig. 12 Analytical buckling loads of hemispherical shells with or without a circular apical cutout under varied ring loads of line type.

of a ring load of line type. Both the slopes before buckling and the buckling loads increased as the diameter of the ring load increased. This behavior is similar to the results obtained by Cagan and Taber[11] for elastic hemispherical shells of D/t in the range 12–16. The corresponding buckling loads F_b and displacement at buckling w_b are shown in Figs. 12 and 13 for varied ring loads of line type. They were made dimensionless with factors $2Et^3/D$ and t, respectively. According to Fig. 12, the buckling loads increased as the diameters of the loading ring increased. Shells without a circular apical cutout

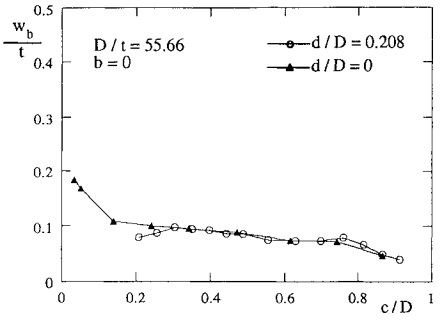

Fig. 13 Analytical displacements at buckling for hemispherical shells with or without a circular apical cutout under varied ring loads of line type.

($d/D = 0$) are special cases of shells with diminishing cutout, and their results show a trend similar to those with cutout. However, no limit buckling occurred for shells without an apical cutout under a ring load of line type when the diameter of the ring load was less than 5.03 mm ($c/D < 0.0349$). Figure 13 shows that the corresponding displacements at buckling were less than 1/10 the shell thickness and varied slightly as the diameter of the ring load increased. The results for shells without cutout show a similar trend except at the region near the apex and are included for comparison.

Conclusions

The buckling and postbuckling behavior of elastoplastic hemispherical shells with circular apical cutout under ring load was investigated analytically and experimentally. For the cases studied, we draw the following conclusions.

1) To have accurate buckling and postbuckling response, the elastoplastic behavior must be considered for relatively thicker spherical shells.

2) A convex postbuckling mode occurred for thin shells and for shells with a ring load of large diameter and a small apical cutout. Conversely, a concave postbuckling mode occurred for thick shells and shells with a ring load of small diameter and a large apical cutout.

3) The proper dimensionless buckling loads of hemispherical shells increased as the ratio of diameter to thickness of shells increased.

4) The size of the circular apical cutout had little effect on buckling loads for shells under a ring load of strip type. With a ring load model of line type, the buckling loads remained constant and decreased slightly only when the edge of the circular apical cutout was near the ring load.

5) The buckling loads of shells increased as the diameter of the ring load increased.

Acknowledgment

This study was supported by the National Science Council, Taiwan, Republic of China, through Grant NSC83-0401-E007-096. The support is greatly acknowledged.

References

[1]Mescall, J. F., "Large Deflections of Spherical Shells Under Concentrated Loads," *Journal of Applied Mechanics*, Vol. 32, No. 4, 1965, pp. 936–938.

[2]Penning, F. A., "Experimental Buckling Modes of Clamped Shallow Shells Under Concentrated Load," *Journal of Applied Mechanics*, Vol. 33, No. 2, 1966, pp. 297–304.

[3]Bushnell, D., "Bifurcation Phenomena in Spherical Shells Under Concentrated and Ring Loads," *AIAA Journal*, Vol. 5, No. 11, 1967, pp. 2034–2040.

[4]Fitch, J. R., "The Buckling and Post-Buckling Behavior of Spherical Caps Under Concentrated Load," *International Journal of Solids and Structures*, Vol. 4, No. 4, 1968, pp. 421–446.

[5]Brodland, G. W., and Cohen, H., "Deflection and Snapping of Spherical Caps," *International Journal of Solids and Structures*, Vol. 23, No. 10, 1987, pp. 1341–1356.

[6]Nowinka, J., and Lukasiewicz, S., "Symmetric Elements in Geometrical Analysis of Large Deformations of Spherical Shells," *International Journal of Non-Linear Mechanics*, Vol. 26, No. 2, 1991, pp. 151–168.

[7]Loo, T. C., and Evan-Iwanowski, R. M., "Interaction of Critical Pressure and Critical Concentrated Loads Acting on Shallow Spherical Shells," *Journal of Applied Mechanics*, Vol. 33, No. 3, 1966, pp. 612–616.

[8]Holston, A., Jr., "Approximate Analytical Solutions of the Finite-Deflection Equations for a Shallow Spherical Shells," *Journal of Applied Mechanics*, Vol. 34, No. 1, 1967, pp. 65–72.

[9]Taber, L. A., "Large Deflection of a Fluid-Filled Spherical Shells Under a Point Load," *Journal of Applied Mechanics*, Vol. 49, No. 1, 1982, pp. 121–128.

[10]Evan-Iwanowski, R. M., Loo, T. C., and Tierney, D. W., "Local Buckling of Shells," *Developments in Mechanics*, Vol. 2, edited by S. Ostrach and R. H. Scanlan, Pergamon, New York, 1963, pp. 221–251.

[11]Cagan, J., and Taber, L. A., "Large Deflection Stability of Spherical Shells with Ring Loads," *Journal of Applied Mechanics*, Vol. 53, No. 4, 1986, pp. 897–901.

[12]Xie, J. R., Chen, Y. Z., and Ho, D., "Axisymmetric Buckling of Truncated Shallow Spherical Shells," *Computers and Structures*, Vol. 34, No. 2, 1990, pp. 297–301.

[13]Gu, S., "Buckling Behaviour of Ring-Loaded Shallow Spherical Shells with a Centre Hole," *International Journal of Non-Linear Mechanics*, Vol. 26, No. 2, 1991, pp. 263–274.

[14]Gu, S., "Application of ß-Spline Approximation to Symmetric Buckling Problems of Truncated Shallow Spherical Shells Subjected to Line Loads," *International Journal for Numerical Methods in Engineering*, Vol. 31, No. 5, 1991, pp. 895–907.

[15]Bathe, K. J., *Finite Element Procedures in Engineering Analysis*, Prentice–Hall, Englewood Cliffs, NJ, 1982, Chap. 6.

[16]Yeh, M. K., and Wei, C. H., "Collapse Analysis of Elastoplastic Shells," *The Chinese Journal of Mechanics*, Vol. 6, No. 1, 1990, pp. 23–30.

[17]Lin, M. C., and Yeh, M. K., "Buckling of Elastoplastic Circular Cylindrical Shells Under Axial Compression," *AIAA Journal*, Vol. 32, No. 11, 1994, pp. 2309–2315.

[18]Ahmad, S., Irons, B. M., and Zienkiewicz, O. C., "Analysis of Thick and Thin Shell Structures by Curved Element," *International Journal for Numerical Methods in Engineering*, Vol. 2, No. 3, 1970, pp. 419–451.

[19]Owen, D. R. J., and Figueiras, J. A., "Anisotropic Elastoplastic Finite Element Analysis of Thick and Thin Plates and Shells," *International Journal for Numerical Methods in Engineering*, Vol. 19, No. 4, 1983, pp. 541–566.